ORIGINAL ARTICLE

Catalytic oxidation of bis (2-chloroethyl) ether on vanadia titania nanocatalyst

Keshav Chand Soni [a],*, S. Chandra Shekar [b]

[a] *Department of Chemistry, JECRC University, Jaipur 303905, India*
[b] *Defence R&D Establishment, Jhansi Road, Gwalior 474002, India*

Abstract Catalytic oxidation of bis (2-chloroethyl) ether (CEE) was carried over 6 wt.% nanocatalyst (VTN) in the presence of ozone. The VTN was prepared by sol–gel method, while the impregnated catalyst (VTI) was prepared for the sake of comparative study. The catalysts were characterized by BET-SA, CEE-TPD, NH_3-TPD, H_2-TPR, XRD, SEM EDAX and TEM analyses. TPR and TPD data reveal that more acid and redox site was observed on nanocatalyst compared to that of conventional catalyst. The Brønsted acid sites were relatively more on nanocatalyst which were responsible for the higher ozone decomposition at low temperatures. The effects of O_3/CEE ratio, reaction temperature, gas hourly space velocity (GHSV) and relative humidity (RH) were also investigated. The nanocatalyst exhibited the better performance, at low temperature (150 °C) with high selectivity to carbon oxides. The transmission electron microscope data reveal that the sol–gel catalysts' average particles size was 14. At 10% of RH, the complete conversion of CEE into carbon oxides was observed for nanocatalyst at 100 °C with long-term stability. The ozone decomposition data reveal that the particle size and acidity had significant influence up to 100 °C, whereas the thermal effects are predominant over the particle size above 150 °C. A plausible reaction mechanism was proposed based upon the experimental data.

© 2017 The Authors. Production and hosting by Elsevier B.V. on behalf of King Saud University. This is an open access article under the CC BY-NC-ND license (http://creativecommons.org/licenses/by-nc-nd/4.0/).

1. Introduction

Chlorinated ethers are widely used in an array of industrial, agricultural applications, and many cases, which are reported as environmental pollutants. Among the chlorine-containing ethers, CEE was classified as a probable toxic and potential carcinogen in nature (Lingg et al., 1979). It was commercially used as a solvent for fats and greases, a textile cleaning fluid, an ingredient of paints/varnishes, and an intermediate in pesticide production (Lingg et al., 1979). Various treatment processes such as absorption, adsorption, incineration, and thermal oxidation are used to abate the industrial waste gases emission meet the regulatory norms. Owing to the high toxicity of chlorinated ethers, the catalytic oxidation over supported and unsupported metal oxides is mostly cited process to control the emissions (Weller et al., 2010; Krishnamoorthy et al., 2000; Stenger et al., 1993; Padilla et al., 1999; Petrosius et al., 1993). In contrary, these catalysts are reported to deactivate when employed in the degradation of halogenated organics (Padilla et al., 1999; Petrosius et al., 1993) and it is opined that vanadia/titania catalyst is effective for the degradation of chlorinated organics (Wang et al., 2007; Krishnamoorthy et al., 1998). It has been reported that the degradation of 2,4,6-trichlorophenol (TCP) over the vanadia/titania catalysts is primarily

affected by the competitive adsorption of TCP and water. The degradation is also affected by the surface reactions of hydroxyl groups with Cl^- species and adsorbed chlorinated organics (Lomnicki et al., 2003). In the previous study it has been described that above 90% of CEE degradation is achieved at 300 °C and GHSV of 19,000 h^{-1} over 6 wt.% of vanadia–titania (Shekar et al., 2011). But, the effective temperature for catalytic oxidation of chlorinated organics over vanadia/titania is generally above 200 °C, which leads to the dramatic increase in the operating cost. Owing to the environmental concern, the technologies available for the degradation of chlorinated organic at low temperature (<200 °C) are still debatable.

Catalytic oxidation with ozone offers a low-temperature process solution to achieve higher reaction rates compared to that of oxygen (Soni et al., 2014; Shekar et al., 2009; Oyama, 2000; Almquist et al., 2007; Wang et al., 2011; Wang et al., 2009). A previous study has been pointed out that ozone decomposition over a catalyst plays an important role in oxidation process and manganese oxide has the higher activity for ozone decomposition among the p-type transition metal oxides (Oyama, 2000). In another study, the maximum activity of V_2O_5/TiO_2 catalyst for methanol oxidation is reported at 150 °C with gas hourly space velocity of 60,000 h^{-1} (Almquist et al., 2007). It has been reported that the monochlorobenzene conversion over Fe_2O_3 catalyst is only 3% in the presence of air and it is significantly increased to 91% in the presence of ozone at 150 °C. The activation energy for catalytic oxidation of chlorobenzene over iron oxide nanocatalyst is reported to be 20, and 43 kJ mol^{-1} in the presence of ozone and air, respectively (Wang et al., 2011). On the other hand, polychlorinated hydrocarbon oxidation over iron or manganese oxide catalysts, the destruction efficiencies are reported above 90% in the presence of ozone at 180 °C, while in the absence of ozone it is less than 25% (Wang et al., 2009). The addition of ozone significantly enhanced the activity of iron oxide nanocatalyst for the oxidation of dimethyl sulfide at low temperature (<150 °C) (Soni et al., 2015).

In recent years, the supported metal oxide nanoparticles have attracted a great attention due to their small particle size, high surface area, and more closely populated surface coordinatively unsaturated sites, which provide more catalytic reactive sites compared to those of larger particles (Kamat and Meisel, 2002; Iwasaki et al., 1998). Vanadia/titania catalyst seems to be quite superior to other alternatives due to their close crystallographic fit between the (010) plane of V_2O_5 and the (010) and (001) planes of anatase titania, which leads to the epitaxial growth of the vanadia (010) plane to the monolayer level (Reddy et al., 1994). It has been reported the unusual behavior of anatase-supported vanadia ascribed to the formation of a vanadium oxide monolayer at the interface and the isolated monomeric vanadia species, which are active for the oxidation reaction (Kryukova et al., 2003; Christodoulakis et al., 2004). It has also been described that the nanoparticles of V_2O_5 over titania could reduce NO_x with higher activity for prolonged operations (Kristensen et al., 2011). For obtaining more active and selective vanadia nanoparticles, the high dispersions of vanadium oxide species on support at optimum vanadium loadings are often desirable. In our earlier studies the monolayer formation is achieved at 6 wt.% of vanadium on titania support prepared by the impregnation method, which is more efficient with multiple sites for CEE oxidation (Shekar et al., 2011). In the impregnation method, the vanadium ions remain on the surface of titania support, whereas for sol–gel synthesis, vanadium ions can form active sites at both on the surface and in the support lattice (Rodella and Masteralo, 2003). Hence, the catalytic properties of vanadia catalyst strongly depend upon the preparation method besides the structures of titania, vanadium loading, temperatures, pH of the solution, etc. (Satsuma et al., 2002). The metal alkoxide precursors are used in the conventional sol–gel method where a very critical control over the preparation parameters is required to obtain a homogeneous and transparent gel (Maurya et al., 2005). Due to the moisture sensitive nature of metal alkoxides, a very dry solvent is also required for avoiding the precipitation of hydroxide. Metal peroxides are comparatively easier to prepare with proper precautions as they can be decomposed easily at

lower temperatures compared to their respective oxides. It has been reported that titania catalysts are synthesized by sol–gel procedure using titanium peroxides, which led to high surface area titanium oxide. The addition of hydrogen peroxide to the vanadium pentoxide forms peroxovanadic acid, and upon mixing this with the peroxotitanate solutions, they form a transparent homogeneous viscous gel, which produces a uniformly dispersed vanadia on titania support (Sonawane et al., 2002).

In this study, a sol–gel procedure is used for the synthesis of the vanadia/titania nanocatalyst, and conventional catalyst is prepared by the wet impregnation method with same vanadium loading. The resulting catalysts are tested for the oxidation of CEE using ozone as an oxidant. The purpose of this study was to compare the effect of particle size, on catalytic oxidation of CEE as well as process parameters, which controls the product selectivity. The study also describes significance of particle over wide temperature range, when ozone is employed as an oxidant for mineralization of CEE.

2. Experimental

2.1. Preparation of catalysts

Vanadia/titania nanocatalyst was prepared by sol–gel procedure using vanadium pentoxide (Aldrich, 99.99%) and titanium isopropoxide (Aldrich, 99.9%) as vanadium and titanium precursors, respectively. Titanium isopropoxide (6.67 g) was dissolved in 50 ml isopropanol in a round-bottom flask and then it was added dropwise into 30 ml of hydrogen peroxide (30%) with constant stirring at 3 °C and a transparent orange sol of peroxotitanate complex was obtained. The vanadium pentoxide (0.425 g) was dissolved in 25 ml aqueous ethanol solution, and 10 ml of H_2O_2 was slowly added (ice bath at 3 °C by monitoring the pH 3 to 4) to get a clear orange solution and steadily it turns to deep red color by formation of peroxovanadic acid. This peroxovanadic acid solution was gently added to the peroxotitanate complex solution. The pH of the above solution was maintained at 1.2 by adding of glacial acetic acid (Aldrich, 99.8%) and constant stirring at 3 °C for 1 h. A transparent homogeneous yellow viscous gel was formed, which was dried at 120 °C for 12 h followed by calcination at 350 °C for 6 h in air and was designated as nanocatalyst (VTN), containing 6 wt.% of vanadium. For the sake of comparison, another vanadia/titania catalyst was prepared by the wet impregnation method. The peroxovanadic acid solution was prepared using identical method described for sol–gel procedure. However, this solution was added drop wise to impregnate the TiO_2 support (1.9 g, Aldrich, BET-SA 59 m^2/g) under constant stirring by following the similar procedure. The excess solvent was removed, and then dried at 120 °C for 12 h followed by calcination at 350 °C for 6 h in air and was designated as conventional catalyst (VTI), containing 6 wt.% of vanadium.

2.2. Catalyst characterization

The BET specific surface area and pore size distribution of the calcined catalysts were measured with a Micromeritics, ASAP2020 instrument using a nitrogen adsorption at −196 °C. Prior to analyses, 0.2 g of the catalyst was loaded into a reactor and degassed at 120 °C with for 1 h. X-ray diffraction patterns (XRD) of calcined catalysts were recorded on a Rigaku diffractometer using Ni-filtered Cu K_α radiation ($\lambda = 1.5406$ Å). The Scanning electron microscopy (SEM)

and energy dispersive X-ray analyses (EDAX) were carried out on a JEOL JAX-840 EEM. Transmission electron microscope (TEM) images of the catalysts were obtained using a JEOL JEM-200FX microspore at 200 kV. The TEM sample was prepared by putting a few droplets of a colloidal suspension of the catalyst in acetone on a copper grid coated with a thin carbon film. The sample was dried and kept in a vacuum oven in desiccators before putting them in the sample holder. Temperature programmed reduction (TPR) and desorption (TPD) were conducted on the TPD/Pulse chemisorption unit (Nuchrom Technologies, India) unit equipped with a thermal conductivity detector. TPR studies of the catalyst sample (0.1 g) were carried out using a 5% H_2–Ar mixture (50 cc/min) at a constant heating rate (10 °C/min, up to 700 °C).

The CEE was allowed to adsorb on 0.1 g of catalyst at 30 °C under comparable reaction conditions in the absence of any oxidizer for 1 h and charged into the quartz reactor for thermal desorption studies. TPD of CEE was performed by heating the sample from 30 to 500 °C at a rate of 10 °C/min in helium as carrier gas. In the TPD of NH_3 experiments, the catalyst sample was saturated by flowing ammonia (1500 ppm, NH_3/Ar) gas at 100 °C. The temperature was then increased from 100 °C to 700 °C at a rate of heating 10 °C/min in helium flow (50 cc/min). The nature and strength of the acid sites of the catalyst were determined by NH_3 adsorption studies using Perkin Elmer 65 FT-IR spectrophotometer using the Harrick assembly. The sample was placed in the Harrick cell and heated to 400 °C in N_2 flow (2 h). It was cooled to 100 °C and NH_3 was adsorbed on the catalyst sample. The spectra were recorded at 100 °C and the spectrum of the neat catalyst (before NH_3 adsorption) was subtracted from the spectra for qualitative and quantitative analysis.

2.3. Catalytic activity measurements

CEE activity measurements were performed in a fixed-bed reactor (12 mm ID 30 mm length) using 0.2 g catalyst (powder form) diluted with glass beads between two layers of quartz wool and were placed in an electrically heated tubular furnace (Kartik Instrumentation). The temperature inside the reactor was measured and controlled through West 6400 with K-type thermocouple, which was placed at center of the catalyst bed and initially the catalysts were activated at 120 °C in N_2 (50 cc/min) for an hour. The CEE (Aldrich, 99%), and N_2 and O_2 (Baruka Gases, India Ltd., 99.8%) gases were used in this study. A precise infusion pump (KD Scientific 2000) is used to maintain the CEE flow rate (0.1 ml/h). To avoid condensation of feed mixture, all the lines were preheated before entering to the reactor at 140 °C. The reaction was studied in the temperature range of 50–200 °C, with gas hourly space velocities (GHSV) from 12,000 to 30,000 h^{-1}. The ozone to the CEE mole ratio was varied from 0.5 to 2, and the CEE concentration was fixed at 600 ppmv. A temperature-controlled humidifier was used to maintain the relative humidity (RH %) and the N_2 flowing through the humidifier was directly mixed with the reactor inlet stream. The RH% was measured by using the RH sensor equipped with digital transmitter (Abacus Technologies, USA) expressed as RH at the given temperatures. The desired relative humidity (RH) was adjusted by varying the carrier gas flow and humidifier temperature.

The ozone generator was standardized by the iodometric method (Richard, 1993). The flow rates of oxygen through the ozone generator, nitrogen, and CEE in N_2 were adjusted using mass flow controllers (Sierra Instruments). The product mixture was adsorbed in traps containing acetonitrile cooled to −5 °C. The bypass line and effluent stream temperature were kept at 100 °C, allowing for the analysis of the gas stream prior to the reactor. The non-condensable phase was passed through (SR-94 electrochemical based), CO_2 (IR based detector P-90 Technovation Analytical Instruments, India) sensors for carbon oxide analyses. The condensable phase was analyzed by the Varian 450-GC equipped with FID/PFPD detector. Qualitative analysis was done by Agilent GC-MS (6890N) equipped with mass-selective detector using BP10 (30 M × 0.25 mm) column. Acetaldehyde, chloroacetaldehyde, formic acid and acetic acid were observed as partial oxidation products (POP) at a lower temperature whereas carbon oxides (CO_x) hydrochloric acid and acetaldehyde were the major products at the higher temperatures.

3. Results and discussions

3.1. BET surface area

The vanadia/titania nanocatalyst has significant higher surface area (205 $m^2 g^{-1}$) than the impregnated catalyst (52 $m^2 g^{-1}$). The formation of vanadia xerogel on titania due to the gelation by mixing of peroxovanadic acid, and peroxotitanates are the responsible factors for an increase in surface area of nanocatalyst (Alonso and Livage, 1999). It is obvious that the surface area of impregnated catalyst was lower compared to that of titania support, which is due to the impregnation vanadia on the support (Oliveira et al., 2006). Adsorption and desorption isotherms for both the catalysts are depicted in the Fig. 1a inner figure. The nitrogen adsorption isotherms of VTN catalyst reveal a little rise at a low relative pressure (P/P^0 from 0.02 to 0.08), reflecting the abundance of mesopores structure, while a very slight rise at high relative pressures ($P/P^0 \leqslant 1$) may be due to adsorption takes place mainly on the outer surface, and in the macropores.

The narrow range of pore size distribution is observed on both the catalysts (Fig. 1a), and most of the pores are mesopore, which is ascribed to the TiO_2 support. The average pore volume and pore size of the nanocatalyst (0.29 $cm^3 g^{-1}$ and 206 Å, respectively) is higher than that of impregnated catalyst (0.07 $cm^3 g^{-1}$ and 160 Å). One of the findings shows that vanadium and titanium peroxides decompose to their respective metal oxides with the evolution of oxygen, which increases the mean pore diameter of nanocatalyst and makes more porous (Maurya et al., 2005).

3.2. X-ray diffraction

The absence of V_2O_5 diffraction signals (Fig. 1b) in nanocatalyst may be due to reduced nucleation of vanadia particle, which is an indication of high disperse state of vanadia. In contrast, the presences of diffraction signal at $2\theta = 20.26°$ in impregnated catalyst indicate the formation of larger particles of polymeric/three dimensional vanadia clusters on titania (Kristensen et al., 2011). Similar observations are reported for vanadia nanocatalyst by using NH_4Cl as crystallization
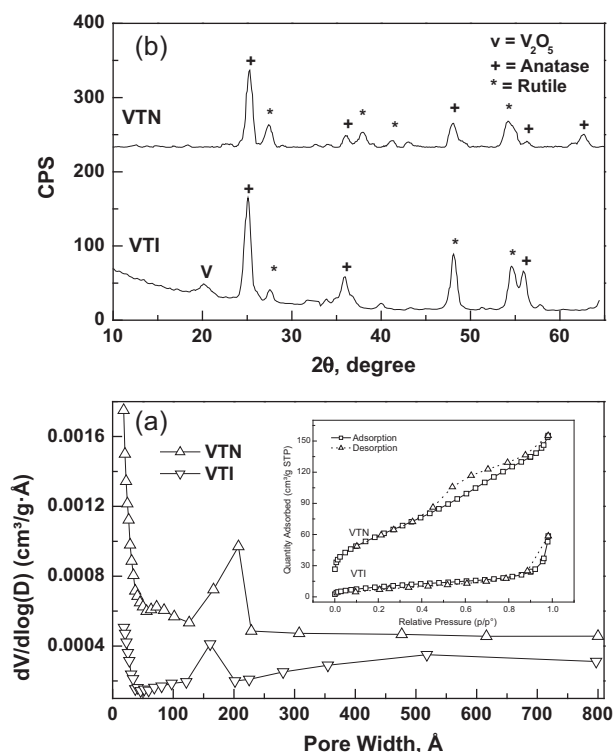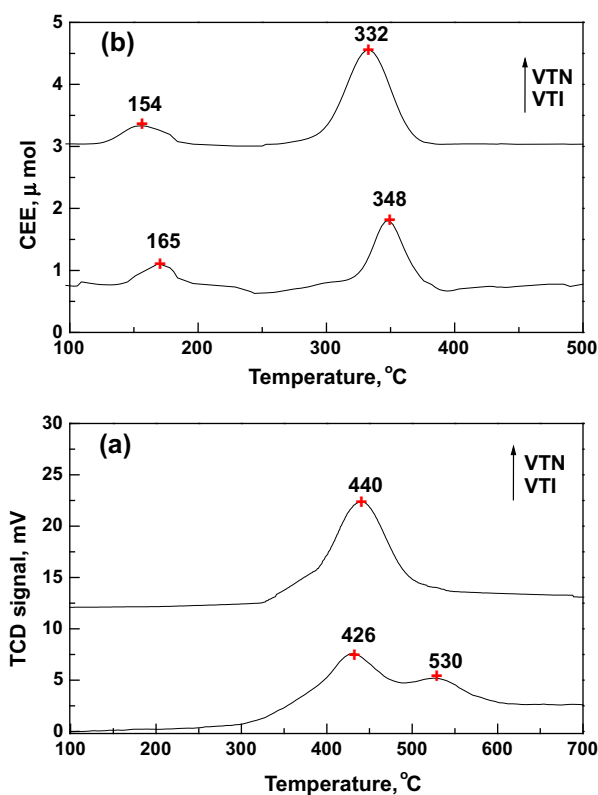
Figure 1 (a) Pore size distribution of the catalysts, inner figure is adsorption and desorption isotherm. (b) X-ray diffraction patterns of the catalysts.

Figure 2 (a) Temperature programmed reduction profile of the catalysts. (b) Temperature programmed desorption profile of CEE over catalysts.

seed (Kruse et al., 2009). In the present study, no evidence of crystalline V_2O_5 is noticed, which indicates that nanocatalyst can accommodate more vanadia than that of impregnated catalyst without forming crystalline vanadia (Bulushev et al., 2000). The diffraction signals at $2\theta = 25.28°$ and $27.5°$ correspond to the diffraction planes of (1 0 1) of anatase and rutile titania, respectively (ASTM# 86-1157) (Sonawane et al., 2002). The relative intensities of titania diffraction signals are weaker for nanocatalyst compared to the impregnated catalyst.

3.3. Temperature programmed reduction (TPR) and TPD of CEE

Temperature-programmed reduction profiles (Fig. 2a) of nanocatalyst showed a single peak with a maximum at 440 °C which is associated with highly dispersion of isolated monomeric vanadia species, which is reduced in a single step from V^{5+} to V^{3+} (Lee et al., 2005; Boningari et al., 2013). There is no high temperature reduction peak (above 500 °C) observed for nanocatalyst, which indicates the absence of crystalline vanadia phase on titania support which is in line with the observations of X-ray diffraction data. The impregnated catalyst indicated multi step reduction pattern with a sharp peak at about 426 °C corresponds to the reduction of V^{5+} to V^{4+}, and the second broad peak centered at 530 °C is related to the reduction of V^{4+} to V^{3+}. The presences of two reduction peaks are associated with the monomeric as well as the polymeric vanadia species, which indicates that the vanadium species are heterogeneous (Machold et al., 2008; Danilevich

et al., 2014). The hydrogen consumption for reduction peaks at different temperatures is given in Table 1. The relative hydrogen consumption (peak area) of nanocatalyst also confirms the presence of more redox sites, which correspond to the fine distribution of the vanadia. The XRD and TPR results reveal that the sample prepared by sol–gel method produced different structural characteristics than the impregnation.

The TPD of CEE data reveals the multi step desorption pattern for both the catalysts (Fig. 2b). The low temperature peak for VTI catalysts, T_{max} at 165 °C is ascribed to desorption of physisorbed CEE, which corresponds to the maximum catalytic activity in ozone at 150 °C. The high temperature (HT) peak at 348 °C is attributed to desorption of strongly chemisorbed CEE as well as thermal decomposition of CEE on the vanadia active sites. It is observed the shifting of desorption peaks toward the lower temperature for nanocatalyst, which may be attributed to the small size of vanadia particles. The HT peak area is more for nanocatalyst due to the higher population of vanadia redox sites as compared to that of impregnated catalyst.

3.4. Temperature programmed desorption (TPD) of ammonia

The TPD profiles of ammonia show that the overall acidity is higher for nanocatalyst compared to the impregnated catalyst (Fig. 3a). It is interesting to note that, a shoulder peak at T_{max} at 240 °C and a sharp peak at 300 °C indicate the presence of two type's acidic sites in nanocatalyst (Sun et al., 1997). On the other hand impregnated catalyst shows the single symmetric

Table 1 Catalytic properties of the VTI and VTN catalysts.

Catalyst	Theory (wt.%)	V (at.%)	V (at.%/m^2)	BET SA (m^2/g)	TPR Peak 1		TPD NH$_3$ Acidity	Spec. Acid	Ozone TOF[a]	XRD	TEM nm
					T_{max} (°C)	H$_2$ (ml/g)	μ (mol/gc)	μ (mol/g/m^2)			
VTI	6	3.09	0.62	52	434	7.5	27	0.51	121	A & R	42
VTN	6	3.02	0.60	205	440	15.9	48	0.23	363	A & R	12

A = Anatase, R = Rutile.
[a] % Ozone decomposition/specific acidity.

peak centered at 254 °C ascribed to the acidic sites with more homogeneous distribution reflecting the TiO$_2$ surface (Maurya et al., 2005). Fourier transform infrared (FTIR) studies of ammonia desorption are illustrated in Fig. 3b, which shows the peak at 1433 cm^{-1} of Brønsted acid sites and at 1603 cm^{-1} of Lewis acid sites. The coordinatively unsaturated surface (CUS) vanadium cations, forming Lewis acids, can adsorb ammonia, while ammonium ions are formed on surface V—OH as well as Ti—OH Brønsted acid sites. Similar observation has been reported by Chen et al. for the V$_2$O$_5$/TiO$_2$ catalyst prepared by the impregnation method (Chen et al., 2011).

The observed broadness of this peak suggests the presence of Lewis acid sites of different strength. Though the acidity is independent of V$_2$O$_5$ content, which appears to have indirect influence on specific acidity, total acidity increases due to the increase in surface area (Kristensen et al., 2011). It has been reported that ammonia desorption from Brønsted acid sites occurs at lower temperatures compared to Lewis acid sites because adsorption of NH$_3$ was more weakly on Brønsted acid

sites compared to that of Lewis acid sites (Snark et al., 1992). The amount of desorbed ammonia is higher for nanocatalyst (48 μmol g^{-1}) than that of impregnated catalyst (27 μmol g^{-1}). However, the specific acidity (VTN 0.234 and VTI 0.509 μmol m^{-2}) is much higher for the impregnated catalysts which indicate the acid site density is relatively more for the impregnated catalyst. It is opined that the presence of more acid sites and better dispersion of vanadia nanoparticles enhanced the catalytic activity.

The TPD and TPR results reveal that the impregnated catalyst is more uniform with respect to acidity whereas they are diverse with respect to redox behavior. In contrast, the nanocatalyst is more homogeneous with respect to redox properties, and the acidic sites are heterogeneous in nature. The heterogenic acidity in the case of nanocatalyst is attributed to the sol–gel procedure, which reflected in the surface properties contributing from both the support and active vanadia sites.

3.5. SEM-EDAX and TEM analysis

The SEM micrograms of VTI and VTN catalysts are shown in Fig. 4a and b, respectively and the surface atomic percentage obtained by EDAX analysis is presented in Table 1. The impregnation method provided a visible nonuniform surface which is due to the formation of V$_2$O$_5$ clusters on the surface of TiO$_2$, whereas the nanocatalyst exhibits relatively more homogeneous and fine pore morphology. The TEM micrographs of VTI and VTN catalysts are shown in Fig. 5a and b, respectively. The vanadia particles in VTI catalyst are wider distributions with agglomerated irregularly shaped particles. In contrast, catalyst prepared by sol–gel method is produced as more homogeneous and well-dispersed vanadia nanoparticles with a narrow particle size distribution. A well-dispersion of V$_2$O$_5$ in Al$_2$O$_3$ matrix is reported for nanocatalyst prepared by a micro arc oxidation method, and the uniform distributions of V$_2$O$_5$ nanoparticles are noticed in grown layers (Bayati et al., 2010). The particles size distribution of VTN and VTI catalysts is displayed in Fig. 6a and b, respectively. The catalyst synthesized by the impregnation method shows the average particle size of 42 nm, and majority of the particles are in the range of 25–55 nm (Lee et al., 2005; Snark et al., 1992). On the other hand, nanocatalyst prepared by sol–gel method exhibits a very narrow particle size distribution ranging from 8 to 16 nm with a mean size of 12 nm, and the larger particle size of VTI catalyst might be due to the small surface area and wide pore size of support compared with nanocatalyst. The TEM data clearly demonstrate that the sol–gel method produced the smaller vanadia particles with wider distribution and is in line with the observations with the XRD data for nanocatalyst.
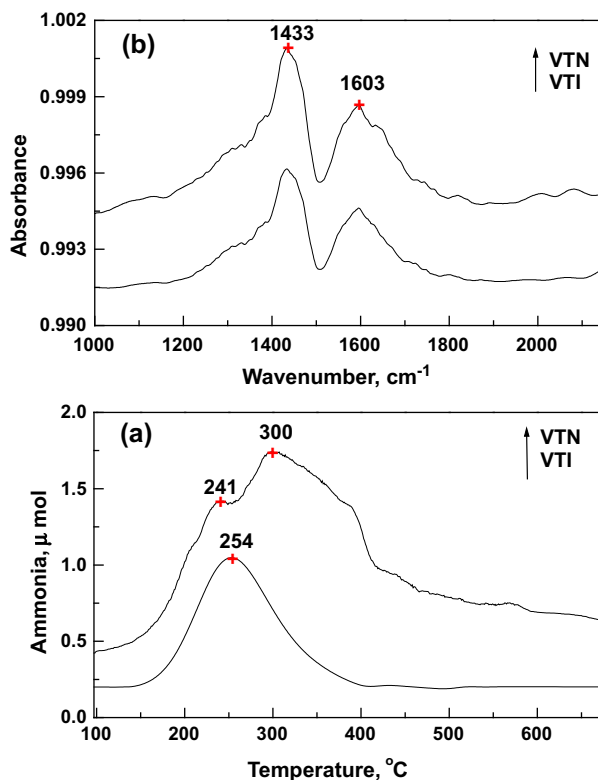
Figure 3 (a) Temperature programmed desorption profile of ammonia over catalysts. (b) FTIR – temperature programmed desorption profile of ammonia over catalysts.
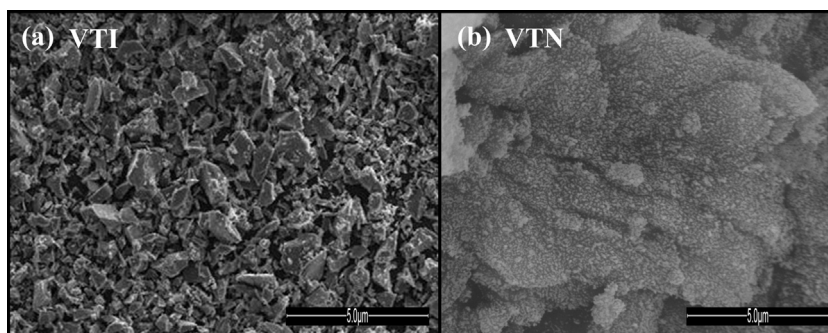
Figure 4 SEM micrograph of the catalysts (a) VTI and (b) VTN.
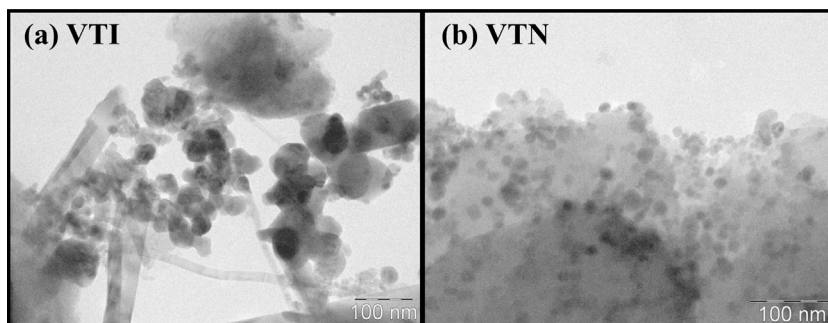
**Figure 5** TEM micrograph of the catalysts (a) VTI and (b) VTN.

4. Activity studies

4.1. Effect of reaction temperature on ozone decomposition

Ozone decomposition studies at various temperatures on both the catalysts are presented in Fig. 7a. The results reveal that the ozone decomposition in the absence of catalyst varies from 17% to 40% with increasing temperature from 50 to 200 °C (Wang et al., 2011; Soni et al., 2015). The ozone decomposition on TiO_2 support varies from 20% to 41% in the temperature range of 50–200 °C. The decomposition of ozone is increased significantly in the presence of a catalyst even at ambient temperatures. The ozone decomposition studies reveal that higher amount of ozone decomposition is observed on nanocatalyst in comparison with impregnated catalyst from 50 to 150 °C which has (a) higher surface area and more active sites observed in TPR and TEM and (b) stronger acidity as well as its population observed by the TPD of CEE and ammonia values for nanocatalyst is responsible for higher decomposition (Demessie and Devulapelli, 2008; Demessie and Devulapelli, 2009). The turnover frequencies of ozone decomposition per site based on the specific acidity for VTN catalyst are three-folds higher than those for VTI catalyst. In contrast, at 200 °C, both the catalysts perform similar decomposition activity. It appears that the decomposition at this temperature is independent of the particle size and the thermal effects are predominant as approaching 200 °C.
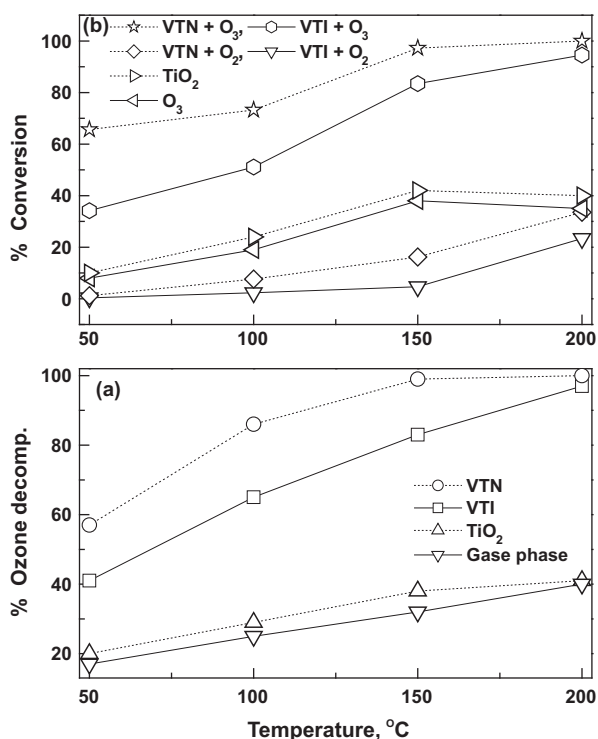
4.2. Effect of reaction temperature on CEE oxidation

The effect of reaction temperature on CEE oxidation is carried out at an O_3/CEE mole ratio of 1 and GHSV of 19,000 h^{-1}
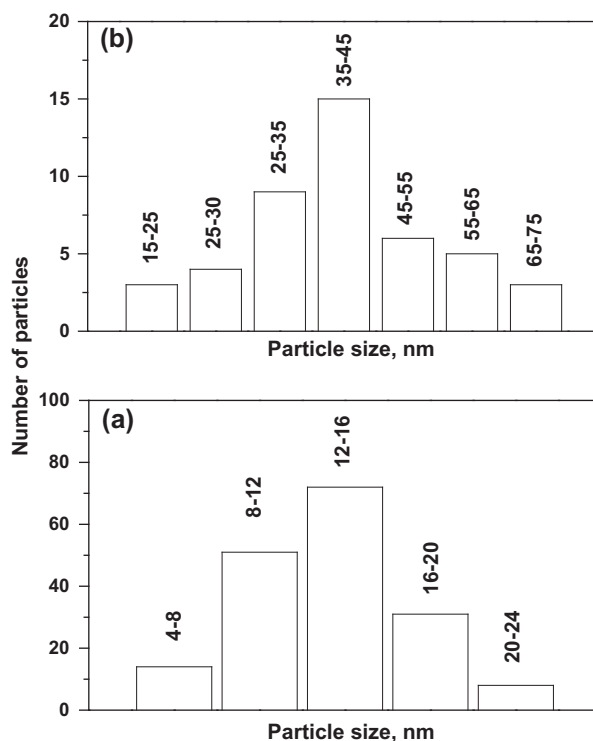
Figure 6 Particle size distributions of the catalysts as obtained from the TEM (a) VTN and (b) VTI.

(Fig. 7b). The conversion values of CEE on both the catalysts are observed less than 35% at 200 °C in the presence of oxygen. A maximum of 38% at 150 °C is observed for the gas
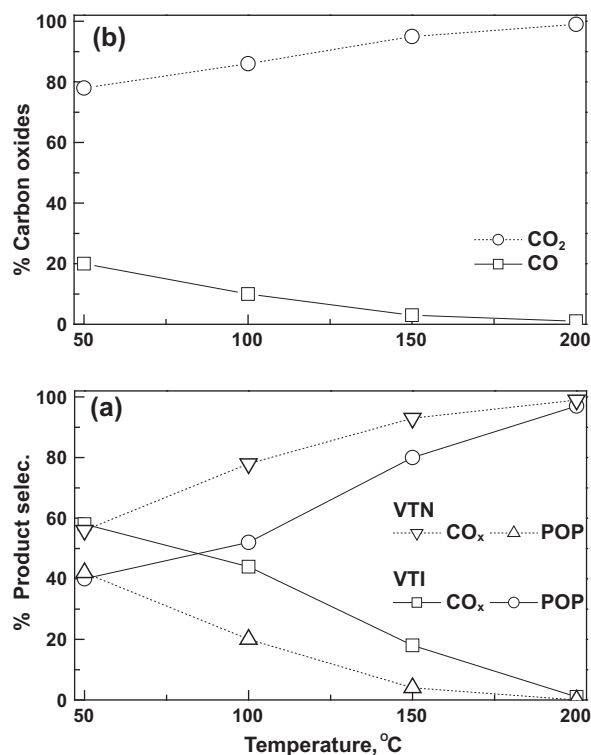
Figure 7 Effect of reaction temperature on (a) ozone decomposition, (b) CEE conversion and GHSV = 19,000 h^{-1} and O$_3$/CEE = 1.

phase ozonation of CEE and further increase in reaction temperature led to decrease in conversion rate due to the thermal decomposition of ozone (Soni et al., 2015). Ozone assisted CEE conversion on TiO$_2$ support is observed 10% at 50 °C and reaching maximum up to 42% at 150 °C. In contrast, for ozone and VTI catalyst, the minimal activity is 34% at 50 °C and goes through a maximum value of 83% at 150 °C. It is noteworthy in mentioning that, when both ozone and nanocatalyst are employed, the conversion value of CEE is about 65% at 50 °C, and reaches up to maximum of 99% at 150 °C. The result confirms the experimental observations that the effectiveness of ozone for CEE oxidation is optimally near to 150 °C. It is observed that both the catalysts performed almost similar activities at 200 °C, which is reinforcing the ozone decomposition studies, that thermal effects are more predominant than the particle.

Identical products are observed on both the catalysts in the presence of ozone (Fig. 8a) with a significant variation in the product selectivity at all the reaction temperatures. The VTI catalyst shows, the selectivity to CO$_x$ is minimum of 42% and goes up to a maximum of 97% at 200 °C. The selectivity to POP is decreased by the rise in reaction temperature. On the other hand, in the presence of nanocatalyst, the CO$_x$ selectivity is observed to be 56% at 50 °C and only the carbon oxides are observed at 200 °C. On the other hand, the selectivity to POP decreased with temperature and at 200 °C there is no notice of POP formation. The nanocatalyst gives high selectivity toward CO$_x$ compared to the VTI catalyst, and no chloride deactivation is noticed in both the catalysts. It has been observed that nanocatalyst contains stronger acid sites, and higher H$_2$ uptake, which in turn reflects the number of

active sites than VTI catalyst. The small particle sizes of vanadia nanoparticles indicate the faster re-oxidation of the active site by ozone, and it increases the complete mineralization of CEE at relatively lower temperatures (Soni et al., 2015). Carbon oxide formation is illustrated as a function of reaction temperature in Fig. 8b. The CO formation is observed to be 20% at 50 °C and decreased with increase in reaction temperature and attained a stable value of 1% at 200 °C. On the other hand the CO$_2$ formation is increased with temperature and attained a stable value of 99%. Though the CO formation is observed at low temperature, it is observed that the CO$_2$ formation is fairly predominant in all reaction temperature ranges.
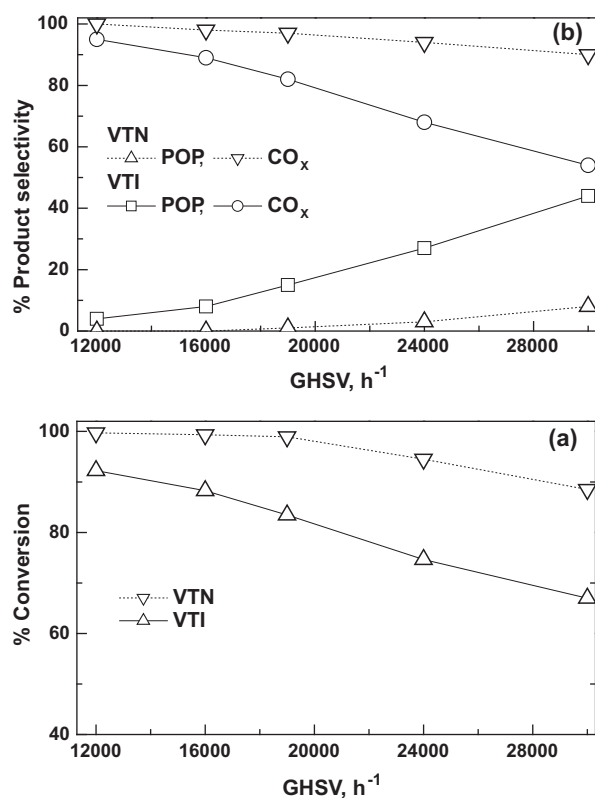
In order to ascertain the combined effect (particle size effect and ozone) on the CEE oxidation, the activation energy is calculated for both catalysts in catalytic oxidation of CEE. In the absence of ozone, the activation energies are 40 kJ mol^{-1} and 46 kJ mol^{-1} for nanocatalyst and VTI catalyst, respectively. On the other hand, in the presence of ozone and catalysts, the activation energy is significantly reduced to 19.6 and 30.8 kJ mol^{-1}, for VTN and VTI catalyst, correspondingly. Thus, the activation energy in the oxidation reaction is considerably reduced when ozone is applied. Similar results are reported for the oxidation of chlorobenzene over Fe and Mn catalysts (20 kJ mol^{-1}) (Wang et al., 2009). Due to the smaller particles of vanadia in nanocatalyst, and the higher acidic sites the activation energy for ozone assisted catalytic oxidation reaction is observed to be twofolds lower than that of the VTI catalyst, which clearly demonstrates the advantage of nanoparticles.

Figure 8 Effect of reaction temperature on (a) product selectivity over catalyst and (b) the formation of carbon oxides over VTN catalysts at GHSV = 19,000 h^{-1} and O$_3$/CEE = 1.

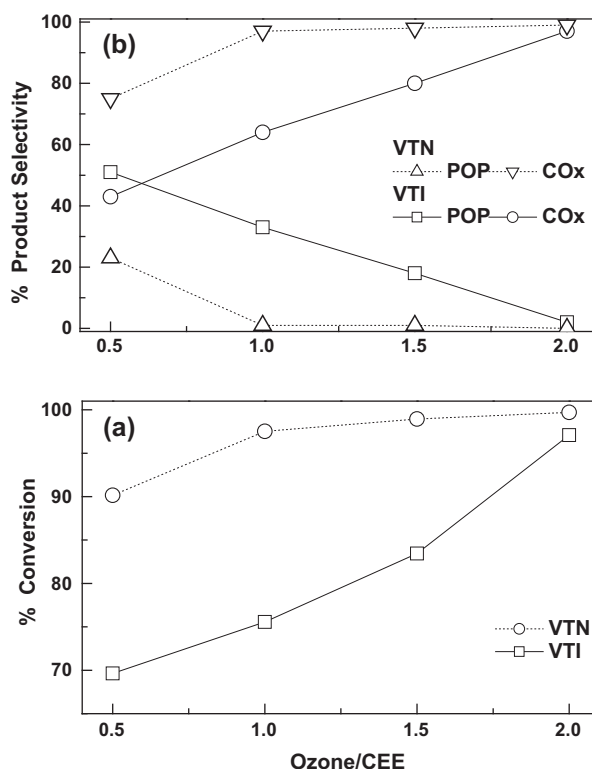## 4.3. Effect of gas hourly space velocity (GHSV) on CEE oxidation

The effect of GHSV on CEE conversion and product selectivity is studied at an O_3/CEE mole ratio of 1 at 150 °C and results are shown in Fig. 9a and b, respectively. The results reveal that the CEE conversion and CO_x selectivity values are decreased by an increase in GHSV from 12,000 h^{-1} to 30,000 h^{-1}. It is observed that, the decrease is less pronounced in the case of VTN compared to the VTI catalyst. In the presence of nanocatalyst, the conversions of CEE and CO_x selectivity are almost 100% in the range of GHSV of 12,000–19,000 h^{-1}. As increasing GHSV up to 30,000 h^{-1}, CEE conversion and CO_x selectivities have decreased to 83% and 90%, respectively. In case of VTI catalyst, the conversion is decreased from 93% to 66% with the increase in GHSV. The selectivity of CO_x is observed to be 95% at GHSV of 12,000 h^{-1} and POP selectivity is about 4%. As increasing GHSV to 30,000 h^{-1}, the selectivity of POP and CO_x over VTI catalyst is around ∼50%. The results reveal that the consecutive reaction to form CO_x is suppressed at higher GHSV, and the overall yields of POP and CO_x remained almost constant. It is well predicted for the catalyst as the surface contact time between reactant and catalyst will decrease with increasing GHSV (Demessie and Devulapelli, 2008). CEE oxidation and product selectivity clearly indicate that the nanocatalyst can perform better activity at higher space velocities, for complete degradation of CEE as compared to the impregnated catalyst.

4.4. Effect of O_3/CEE ratios on CEE oxidation

The effect of O_3/CEE mole ratios (from 0.5 to 2) on CEE conversion and product selectivity is studied at 150 °C and GHSV of 19,000 h^{-1} and results are shown in Fig. 10a and b, respectively. The effects of O_3/CEE mole ratios on conversion of CEE and product selectivity on VTN and VTI catalysts are about 90% and 75%, correspondingly at O_3/CEE ratio of 0.5. As increasing O_3/CEE ratio, nearly complete conversion of CEE is achieved and only CO_x formation is observed. At an O_3/CEE ratio of 0.5, about 70% of CEE conversion is observed on VTI catalyst and almost same POP and CO_x selectivity are observed. As the O_3/CEE ratio increased, CEE conversion and CO_x selectivity are increased and virtually complete conversion of CEE to CO_x is observed for the ratio of 2. On the other hand, for VTN catalyst, the formation of POP is completely minimized at an O_3/CEE ratio about 1, which is attributed to the presence of nanosized vanadia in addition to decomposition (ozone TOF are threefolds higher) of ozone for the VTN catalyst. In general, at lower ozone to CEE molar ratio, the formation of POP is predominant whereas the higher ratio favors CO_x formation. The selectivity of POP is significant for VTI catalyst compared to the VTN catalyst. The higher redox sites, offer more to contact areas and in turn the nanocatalyst provides more atomic oxygen species during ozone decomposition and resulted in total oxidation in comparison with the impregnated catalyst at low O_3/CEE ratios (Kim and Shim, 2010).
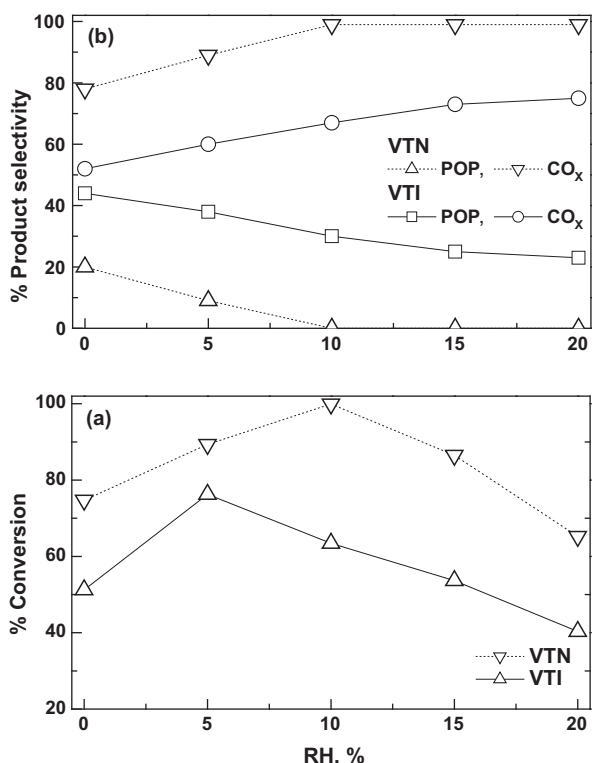

Figure 9 Effect of GHSV on CEE oxidation over catalysts: (a) conversion and (b) product selectivity (Reaction temp = 150 °C and O_3/CEE ratio = 1).

Figure 10 Effect of O_3/CEE molar ratios on CEE oxidation over catalysts: (a) conversion and (b) product selectivity (Reaction temp = 150 °C and GHSV = 19,000 h^{-1}).

4.5. *Effect of relative humidity on CEE oxidation*

The effect of RH (from 0 to 20%) on CEE conversion and product selectivity is conducted at 100 °C and the results are depicted in Fig. 11a and b. The activity of vanadia/titania catalysts for the degradation of CEE is strongly affected by the presence of water vapors. The conversion value of CEE increased from 74% to 99% with RH from 0 to 10% for the VTN catalyst, whereas maximum conversion is observed up to 76% at 5% of RH for VTI catalyst. The results reveal that, with increasing the RH%, the conversion goes through a maximum, and thus further increasing RH to 20%. The conversion is reduced considerably to 65% and 40% for VTN and VTI catalyst, respectively. This is attributed to the competitive adsorption between CEE molecules and water vapors on to the same active sites that reflected in the conversion values at higher RH% (Kryukova et al., 2003). Furthermore, the combined effect of nanocatalyst and ozone has been superior to that of impregnated catalyst because of the more surface hydroxyl groups (acid sites), and vanadia, which easily decomposes ozone to form atomic oxygen/OH for the further reaction with CEE molecules (Kasprzyk-Hordern et al., 2003; Zhao et al., 2012). The selectivity to CO_x for VTI catalyst is observed a minimum of 52% and goes through a maximum of 75% with increasing RH from 0% to 20%. On the other hand, the formation of POP is completely minimized for nanocatalyst and merely CO_x formation is observed at RH of $\geqslant 10$. It is also observed that CO_2 is the only product in the presence of ozone and moisture for VTN catalyst, and no CO is detected in the gaseous products. It is suggested that the increase in the humidity either decreases the CO formation or promotes the extended oxidation of CO by the water gas shift reaction (Demessie and Devulapelli, 2009). Einaga and Ogata reported that the suppression of catalyst deactivation by water vapor greatly promotes the total oxidation of POP to CO_2 as well as facilitates the removal of chloride ion present at the catalyst surface (Einaga and Ogata, 2009).
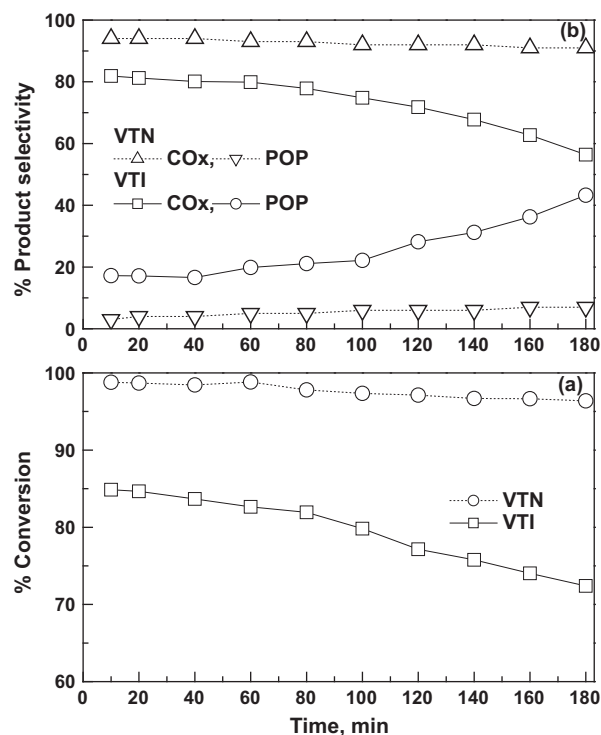
Figure 12 Effects of time on steam on CEE oxidation: (a) conversion and (b) product selectivity (Reaction temp = 150 °C, GHSV = 19,000 h^{-1} and O$_3$/CEE = 1).
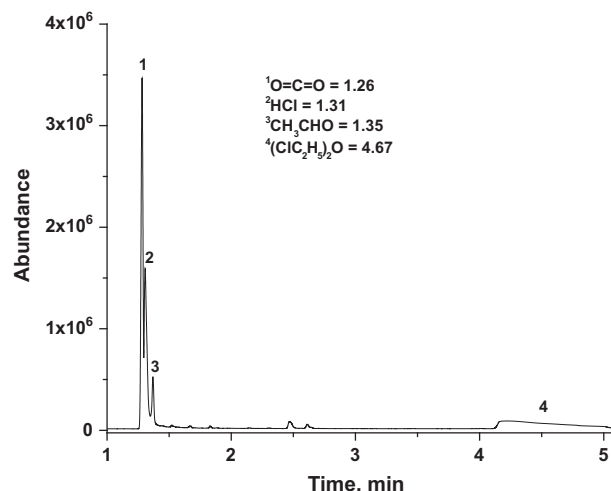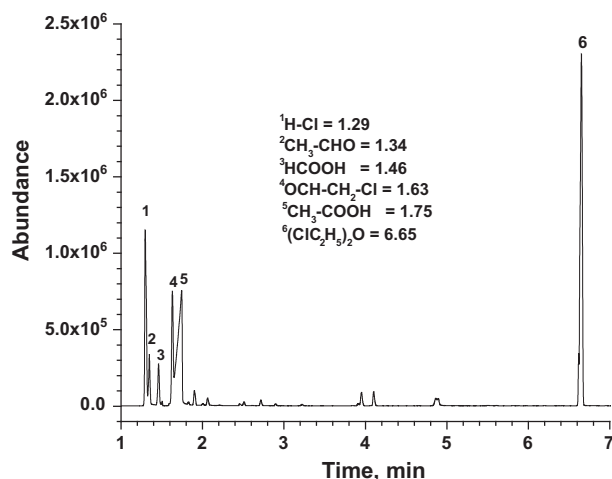
Figure 11 Effect of relative humidity on CEE oxidation over catalysts: (a) conversion and (b) product selectivity (Reaction temp = 100 °C, GHSV = 19,000 h^{-1} and O$_3$/CEE ratio = 1).

Figure 13 GC-MS analysis of non-condensable phase from CEE oxidation over VTN catalyst (Reaction temp = 150 °C, GHSV = 15,000 h^{-1} and O$_3$/CEE = 1).

Figure 14 GC-MS of condensable reaction phase from CEE oxidation over VTN catalyst (Reaction temp = 150 °C, GHSV = 15,000 h^{-1} and O$_3$/CEE = 1).

4.6. Time on stream

Times on stream analysis of CEE oxidation over both catalysts is studied at 150 °C (at O$_3$/CEE ratio of 1 and GHSV of 19,000 h^{-1}) and the results are depicted in Fig. 12a and b. The results reveal that, the nanocatalyst shows a total oxidation of CEE into CO$_x$ and HCl, which exhibited constant activity for nearly three hours. The nanocatalyst shows that CO$_x$ selectivity is almost 100% with time and no deactivation of catalyst is observed for long term operation. The VTI catalyst activity is about 84% in the initial period and attained a steady-state conversion value of 72% in three hours. The selectivity toward CO$_x$ decreased from 81% to 56% in an un-steady state period, whereas the POP formation is minimal or traces

on nanocatalyst. The product selectivity indicates that a fraction of the active sites are deactivated during the initial stage, which is due to the reconstruction of the catalyst surface, and which in turn unable to reactivate with ozone on VTI catalyst (Chu et al., 2003). The study clearly demonstrates that the strong oxidizing power of ozone and vanadia nanoparticles maintains surface active sites, and the steady-state is achieved much faster as compared to the impregnated catalyst.

5. Probable reaction pathway for CEE oxidation

The GC-MS analyses of non-condensable and condensable phase of the reaction product mixture are illustrated in Figs. 13 and 14. A plausible reaction mechanism is described based upon both literature and experimental data (Scheme 1). The total products identified in condensable phase are acetaldehyde, chloroacetaldehyde, formic acid, acetic acid and hydrochloric acid. In the noncondensable phase, HCl, CO, CO$_2$ and acetaldehyde are observed. Overall the acetaldehyde, HCl and CO$_2$ observed as major products in the reactor effluent stream at higher temperature range from 100 °C to 200 °C. It has been acknowledged that decomposition of ozone on supported metal oxide catalysts leads to the formation of highly reactive oxygen species such as superoxide (O$_2^-$) and peroxide (O$_2^{2-}$) species and hydroxyl groups on the surface of the catalyst (Li et al., 2014; Konova et al., 2006). On the other hand, ozone supplies strong oxidation groups than oxygen, which accelerates the catalytic redox cycle at lower temperature and improves the activity of the catalyst itself (Ji et al., 2013). The previous results suggested that an active complex might be formed during ozone decomposition on the transition metal oxides which are capable of oxidizing organic toxic compounds at low temperature (Li et al., 2014; Konova et al., 2006; Ji et al., 2013; Mehandjiev et al., 2001). It is widely accepted that the catalyst surface is reduced when interacting with the reactant, and is subsequently re-oxidized by gas-
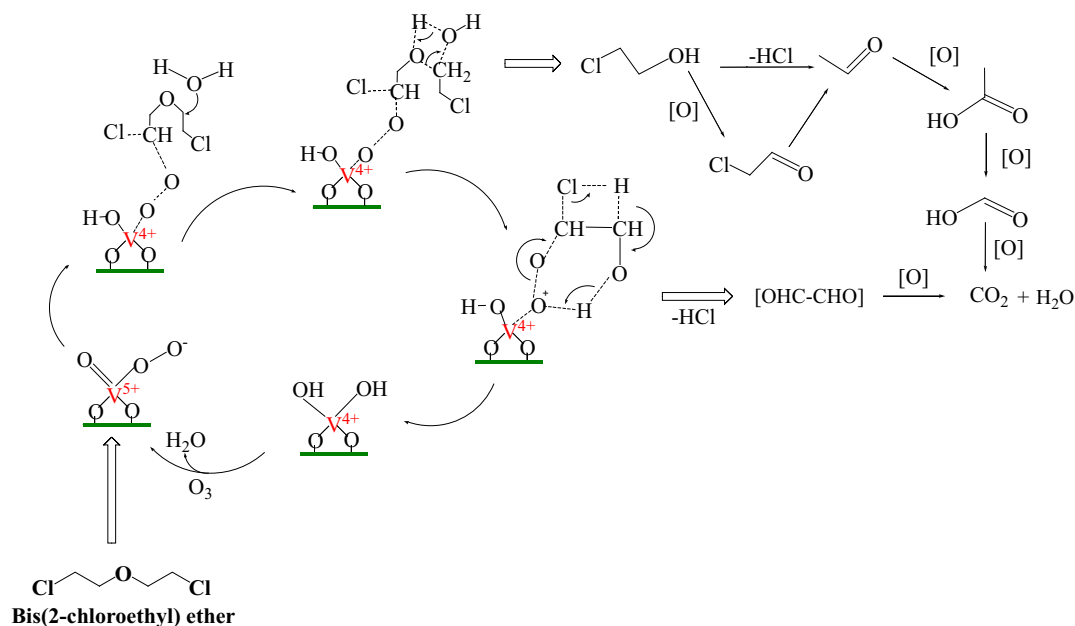
Scheme 1

phase ozone/oxygen in a next step (Gannoun et al., 2011). The process continuously takes place as long as the reactants are present to reduce the catalyst and ozone to re-oxidize the surface. It is proposed that physisorption is the first step in the destruction of pollutants and $V^{5+}O_x$ is considered as the active center of vanadia/titania oxidation catalysts (Ji et al., 2013; Xu et al., 2012). The catalytic data suggest that CEE is adsorbed on the catalyst proceeds by nucleophilic attacks on the chlorine positions (C_β—Cl) via a hydrogen abstraction, and then adsorbed CEE undergoes hydrolytic cleavage (C_α—O) to form chloroethanol assisted by redox/acidic sites. Further, dehydrochlorination of desorbed chloroethanol produces acetaldehyde. Subsequently, chloroethanol oxidizes to chloroacetaldehyde, which will be decomposed into acetaldehyde by dechlorination. The acetaldehyde is readily converted to acetic acid and further extended oxidation leads to the formation of carbon oxides. In the subsequent step, adsorbed chloroethanol undergoes dehydrochlorination with H-abstraction from —C_β—OH to O—V^{4+} surface and breaking of peroxide linkage (C_α—O—O—V^{4+}). The ozone will rupture the —C_α—C_β— bond of glyoxal intermediate and further oxidation produces H_2O and CO_2. The V^{4+}—OH species concurrently formed on the vanadium surface further oxidize via gaseous ozone to complete the catalytic cycle. It is suggested in the alcoholic oxidation the re-oxidation of the vanadium proceeds via adsorption of O_2 at a vacancy site to form a peroxide species (Kilos et al., 2009). This intermediate appears during the catalytic oxidation of CEE over vanadia/titania catalyst in the air-rich condition (Shekar et al., 2011). The formation of $V^{5+}O_x$ species depends on the ozone decomposition ability of a catalyst which is limited by the activity of the sites on the catalyst surface, or the conversion rate of $V^{4+}O_x$ to $V^{5+}O_x$ in time. Xu et al. (2012) have reported that active lattice atoms of oxygen $V^{5+}O_x$ oxidize PCDD/Fs on the catalyst surface so that $V^{5+}O_x$ is reduced to $V^{4+}O_x$; in the presence of oxygen re-oxidation occurs to $V^{5+}O_x$. Higher ozone decomposition on the small size of vanadia particles enhances the catalyst activity, which proceeds the CEE adsorption and oxidative decomposition cycle more quickly at the lower temperatures. On the other hand, the impregnated catalyst still adsorbs CEE, but it is not active enough to treat the amount of CEE gathered on the catalyst. It is concluded that vanadia/titania catalyst is found to be more active in the CEE oxidation, and the activity depends strongly on the preparation method.

6. Conclusions

Catalytic oxidation of CEE with ozone is carried out over vanadia/titania nanocatalyst (VTN) and conventional Impregnated (VTI) catalyst. The results of XRD and TEM indicate that the sol–gel method provided a nanocatalyst with well dispersion of vanadium on titania support. The TPD and TPR results reveal that the nanocatalyst processes more redox and acid sites compared to those of impregnated one. The complete ozone decomposition activity over nanocatalyst at lower temperatures significantly promotes the total oxidation of CEE under comparable conditions. The higher ozone decomposition rate (Ozone TOF) on vanadia nanocatalyst helps the catalyst to oxidize CEE, by enhancing the redox cycle between V^{4+} and V^{5+} in additions to the high acid site distribution. The activity of vanadia/titania catalysts is strongly affected by the presence of humidity, and the optimum humidity is identified to increase the complete mineralization of CEE over VTN catalysts. The particle size effect is insignificant as approaching the reaction temperature of 200 °C. The activation energy

calculated for the nanocatalyst is found to be half of the impregnated catalysts, and the particle size effect is significant for the below 150 °C when ozone is employed as an oxidant. The degraded product such as carbon oxide, hydrochloric acid, acetaldehyde and trace amount of chloroacetaldehyde and chloroethanol is observed, which confirms the proposed degradation path for total and partial oxidation of CEE.

References

Almquist, C.B., Demessie, E.S., Sehker, K.S., Sowash, J., 2007. Environ. Sci. Technol. 41, 4754–4760.

Alonso, B., Livage, J., 1999. J. Solid State Chem. 148, 16–19.

Bayati, M.R., Zargar, H.R., Molaei, R., Golestani-Fard, F., Zanganeh, N., Kajbafvala, A., 2010. Appl. Surf. Sci. 256, 3806–3811.

Boningari, T., Koirala, R., Smirniotis, P.G., 2013. Appl. Catal. B: Environ. 140–141, 289–298.

Bulushev, D.A., Kiwi-Minsker, L., Zaikovskii, V.I., Renken, A., 2000. J. Mol. Catal. 193, 145–153.

Chen, L., Li, J., Ge, M., 2011. Chem. Eng. J. 170, 531T–537T.

Christodoulakis, A., Machli, M., Lemonidou, A.A., Boghosian, S., 2004. J. Catal. 222, 293–306.

Chu, H., Hao, G.H., Tseng, T.K., 2003. J. Hazard. Mater. 100, 301–316.

Danilevich, E.V., Popova, G.Y., Andrushkevich, T.V., Kaichev, V.V., Danilova, I.G., Chesalov, Y.A., Rogov, V.A., Bukhtiyarov, V.I., Parmon, V.N., 2014. Appl. Catal. A: Gen. 475, 98–108.

Demessie, E.S., Devulapelli, V.G., 2008. Appl. Catal. B: Environ. 84, 408–419.

Demessie, E.S., Devulapelli, V.G., 2009. Appl. Catal. A: Gen. 361, 72–80.

Einaga, H., Ogata, A., 2009. J. Hazard. Mater. 164, 1236–1241.

Gannoun, C., Delaigle, R., Eloy, P., Debecker, D.P., Ghorbel, A., Gaigneaux, E.M., 2011. Sol–gel derived V_2O_5–TiO_2 mesoporous materials as catalysts for the total oxidation of chlorobenzene. Catal. Commun. 15, 1–5.

Iwasaki, M., Hara, M., Ito, S., 1998. J. Mater. Sci. Lett. 17, 1769–1771.

Ji, S.S., Li, X.D., Ren, Y., Chen, T., Cen, K.F., Ni, M.J., Buekens, A., 2013. Ozone-enhanced oxidation of PCDD/Fs over V_2O_5/TiO_2-based catalyst. Chemosphere 92, 265–272.

Kamat, P.V., Meisel, D., 2002. Curr. Opin. Colloid Interface Sci. 7, 282–287.

Kasprzyk-Hordern, B., Ziolek, M., Nawrocki, J., 2003. Appl. Catal. B: Environ. 46, 639–669.

Kilos, B., Bell, A.T., Iglesia, E., 2009. Mechanism and site requirements for ethanol oxidation on vanadium oxide domains. J. Phys. Chem. C 113, 2830–2836.

Kim, S.C., Shim, W.G., 2010. Appl. Catal. B: Environ. 98, 180–185.

Konova, P., Stoyanova, M., Naydenov, A., Christoskova, S., Mehandjiev, D., 2006. Catalytic oxidation of VOCs and CO by ozone over alumina supported cobalt oxide. Appl. Catal. A: Gen. 298, 109–114.

Krishnamoorthy, S., Baker, J.P., Amiridis, M.D., 1998. Catal. Today 40, 39–46.

Krishnamoorthy, S., Rivas, J.A., Amiridis, M.D., 2000. J. Catal. 193, 264–272.

Kristensen, S.B., Kunov-Kruse, A.J., Riisager, A., Rasmussen, S.B., Fehrmann, R., 2011. J. Catal. 284, 60–67.

Kruse, A., Kristensen, S., Riisager, A., Rasmussen, S., Fehrmann, R., 2009. J. Mater. Sci. 44, 323–327.

Kryukova, G.N., Zenkovets, G.A., Pfander, N., Su, D.S., Schlogl, R., 2003. Mater. Sci. Eng., A 343, 8–12.

Lee, L.J., Lee, C.H., Lee, S.D., Suh, D.J., 2005. J. Ind. Eng. Chem. 11, 918–925.

Li, J.W., Pan, K.L., Yu, S.J., Yan, S.Y., Chang, M.B., 2014. Removal of formaldehyde over $Mn_xCe_{1-x}O_2$ catalysts: thermal catalytic oxidation versus ozone catalytic oxidation. J. Environ. Sci. 26, 2546–2553.

Lingg, R.D., Kaylor, W.H., Pyle, S.M., Tardiff, R.G., 1979. Toxicol. Appl. Pharmacol. 47, 23–24.

Lomnicki, S., Lichtenberger, J., Xu, Z.T., Waters, M., Kosman, J., Amiridis, M.D., 2003. Appl. Catal. B: Environ. 46, 105–119.

Machold, T., Suprun, W.Y., Papp, H., 2008. J. Mol. Catal. A: Chem. 280, 122–130.

Maurya, S.K., Patil, P., Umbarkar, S.B., Gurja, M.K., Dongare, M., Rudiger, S., Kemnitz, E., 2005. J. Mol. Catal. A: Chem. 234, 51–57.

Mehandjiev, D., Naydenov, A., Ivanov, G., 2001. Ozone decomposition, benzene and CO oxidation over $NiMnO_3$-ilmenite and $NiMn_2O_4$-spinel catalysts. Appl. Catal. A: Gen. 206, 13–18.

Oliveira, P., Cervantes, M.L.R., Ramos, A.M., Fonseca, I.M., Botelho do Rego, A.M., Vital, J., 2006. Catal. Today 118, 307–314.

Oyama, S.T., 2000. Cat. Rev. – Sci. Eng. 42, 279–322.

Padilla, A.M., Corella, J., Toledo, J.M., 1999. Appl. Catal. B: Environ. 22, 107–121.

Petrosius, S.C., Drago, R.S., Young, V., Grunewald, G.C., 1993. J. Am. Chem. Soc. 115, 6131–6137.

Reddy, B.M., Reddy, E.P., Mehdi, S., 1994. Mater. Chem. Phys. 36, 276–281.

Richard, Y., 1993. Ozone Sci. Eng. 15, 465–480.

Rodella, C.B., Masteralo, V.R., 2003. J. Phys. Chem. Solids 64, 833–839.

Satsuma, A., Takenaka, S., Tanaka, T., Nojima, S., Kera, Y., Miyata, H., 2002. Appl. Catal. A: Gen. 232, 93–106.

Shekar, S.C., Soni, K., Bunkar, R., Sharma, M., Singh, B., Nigam, A., Mahato, T., Vijayaraghavan, R., 2009. Catal. Commun. 11, 77–81.

Shekar, S.C., Soni, K., Bunkar, R., Sharma, M., Singh, B., Suryanarayana, M.V.S., Vijayaraghavan, R., 2011. Appl. Catal. B: Environ. 103, 11–20.

Snark, V., Dumesic, J.A., Clausen, B.S., Tornqvist, E., Topse, N.Y., 1992. J. Catal. 135, 246–262.

Sonawane, R.S., Hegde, S.G., Dongare, M.K., 2002. Mater. Chem. Phys. 77, 744–750.

Soni, K., Shekar, S.C., Singh, B., Agrawal, A., 2014. Indian J. Chem., Sect A 53, 484–492.

Soni, K.C., Shekar, S.C., Singh, B., Gopi, T., 2015. J. Colloid Interface Sci. 446, 226–236.

Stenger Jr., H.G., Buzan, G.E., Berty, J.M., 1993. Appl. Catal. B: Environ. 2, 117–130.

Sun, B., Sato, M., Clements, J.S., 1997. J. Electrostat. 39, 189–192.

Wang, H.C., Hwang, J.F., Chi, K.H., Chang, M.B., 2007. Chemosphere 67, S177–S184.

Wang, H.C., Chang, S.H., Chang, P.C., Hwang, J.F., Chang, M.B., 2009. J. Hazard. Mater. 164, 1452–1459.

Wang, H.C., Liang, H.S., Chang, M.B., 2011. J. Hazard. Mater. 186, 1781–1787.

Weller, E.B., Knoll, A., Heberer, T., 2010. Chemosphere 78, 653–658.

Xu, Z.Z., Deng, S.B., Yang, Y., Zhang, T.T., Cao, Q.M., Huang, J., Yu, G., 2012. Catalytic destruction of pentachlorobenzene in simulated flue gas by a V_2O_5–WO_3/TiO_2 catalyst. Chemosphere 87, 1032–1038.

Zhao, D.Z., Shi, C., Li, X.S., Zhu, A.M., Jang, B.W.L., 2012. J. Hazard. Mater. 239–240, 362–369.